GEOPHYSICS, VOL. 72, NO. 5 (SEPTEMBER-OCTOBER 2007); P. SM261–SM271, 16 FIGS., 1 TABLE.
10.1190/1.2736515

Improved applicability of ray tracing in seismic acquisition, imaging, and interpretation

Håvar Gjøystdal[1], Einar Iversen[1], Isabelle Lecomte[1], Tina Kaschwich[1], Åsmund Drottning[1], and Joachim Mispel[2]

ABSTRACT

Ray-based seismic modeling methods can be applied at various stages of the exploration and production process. The standard ray method has several advantages, e.g., computational efficiency and the possibility of simulating propagation of elementary waves. As a high-frequency approximation, the method also has a number of limitations, particularly with respect to a lack of amplitude reliability in the presence of rapid changes of the model functions representing elastic parameters and interfaces. Given the objective of improving the applicability of the standard ray method, we present a strategy that does not require specific extension to finite frequencies. Instead, we define each ray-based process as an element of a system that, as a composite process, is able to obtain better results than the ray-based process applied alone. Other elements of the composite process can be finite-difference modeling or numerical solutions for surface and volume integrals, which are basic constituents of Kirchhoff modeling and imaging. We also include among the process elements recently developed techniques for simulating the migration amplitude on a target reflector and in a local volume, e.g., a reservoir zone. The model is decomposed according to its complexity into volume elements, surface elements, or a combination. The composite process consists of a specified interaction between process elements and model elements, which fits well with the philosophy of modern software design. Model elements that will be exposed to ray-tracing algorithms may need appropriate preparation, e.g., smoothing and resampling. We demonstrate specifically, in a tutorial example, that simulating the seismic response from a reflector by ray-based composite processes can yield better results than applying standard ray tracing alone.

INTRODUCTION

Ray methods have been used extensively in seismology and seismic exploration to study propagation of seismic waves in layered media with varying elastic parameters. In early applications, the focus was mostly on calculating raypaths and traveltimes, referred to as kinematic ray tracing; but throughout the 1970s and 1980s numerical techniques were developed for dynamic ray tracing (Červený and Hron, 1980), which yields wavefront curvature and geometric-spreading attributes. Given certain simplifying assumptions for the model of elastic parameters, one can use such attributes in combination with an approximate zero-order, high-frequency solution of the elastodynamic wave equation (Červený et al., 1977; Červený, 2001) and obtain reliable estimates of P- and S-wave amplitudes. This numerical approach is referred to as the standard ray method, or ray tracing. In the case of applying a point source in the starting point of the ray, we refer to the various attributes calculated by ray tracing (traveltime, amplitude, geometric spreading, etc.) as Green's function attributes. (For a definition of the Green's function, see Aki and Richards, 1980.) The attributes calculated by ray tracing generally are stable if interface normals and gradients of elastic parameters (e.g., P- and S-wave velocities for an isotropic medium) vary smoothly within a region surrounding the ray. This region depends on the dominant seismic frequency and is referred to as the Fresnel volume (Červený and Soares, 1992).

Comparisons with more complete and much more time-consuming techniques such as finite-difference (FD) schemes show that ray-tracing-based theoretical seismograms can be of sufficient quality if the model of elastic parameters is prepared with the necessary smoothness (e.g., Iversen et al., 1996). However, one of the weak-

Manuscript received by the Editor November 30, 2006; revised manuscript received February 20, 2007; published online August 23, 2007.
[1]NORSAR, Research & Development and Applied Seismic Modeling, Kjeller, Norway. E-mail: haavar@norsar.com; einar.iversen@norsar.com; isabelle@norsar.com; tina@norsar.no; aasmund@norsar.com.
[2]Formerly NORSAR, Kjeller, Norway; presently Statoil Research Centre, Postuttak, Trondheim, Norway. E-mail: jmis@statoil.com.

nesses of the standard ray method applied to realistic interpreted geologic structures stems from the fact that the calculations along each ray are superlocal, or quite independent of neighboring rays. A single ray "sees" only the elastic properties and interface behavior exactly along the raypath; thus the stability across the rays depends on the assumption that these parameters are representative of neighboring rays, at least within a Fresnel volume.

Iteration techniques referred to as two-point ray tracing can be used to obtain continuous rays from source to receiver. One such technique is shooting, adjusting the takeoff direction of the ray and retracing until the ray hits sufficiently close to the receiver. Each ray accepted by the iteration process corresponds to an event, i.e., an arrival with a specific traveltime. For complex 3D models, two-point ray tracing can be very time-consuming and can typically miss events in regions with large geometric spreading. This deficiency led to the development of the wavefront construction method (Vinje et al., 1993, 1996a, b; Lambaré et al., 1996), which is more robust than standard ray tracing based on calculation of continuous single rays. The reason for enhanced robustness lies in the fact that a continuous representation of the wavefront, with sufficiently dense sampling of ray points and slowness vectors, is established by interpolation after each time step. In this way, the sampling of parameters influencing the calculation of traveltimes, amplitudes, etc., is adapted to the complexity of the model of elastic parameters. We note, however, that the wavefront construction method only partly solves the problem of lack of ray penetration into shadow zones. Recently, the wavefront construction method has been further developed to include anisotropy (Mispel and Williamson, 2001; Gibson et al., 2005; Iversen et al., 2005).

In the last few years, the number of applications for ray-theory-based methods in seismic exploration (Gjøystdal et al., 2002) has increased. Among the classic applications are generation of synthetic seismograms, calculation of Green's function attributes for Kirchhoff depth migration, and estimation of perturbation quantities for seismic tomography. There are, however, several new applications in seismic modeling, imaging, illumination studies, survey planning, and 4D reservoir analyses. The models used in such contexts are often of a complex nature, including subsalt, overthrust, or gas-cloud geology, which means that the formal validity criteria of the standard ray method (Červený, 2001) may be violated easily.

Similarly, in reservoir studies, particularly when using seismic methods as an analysis tool during oilfield production (4D or time lapse), the models available are generally much too detailed for ray tracing to produce reliable responses. Because of the presence of numerous well logs in the reservoir zone, the models constructed may have details down to the order of 1 m or less. The models may also include faults, pinch-outs, and numerous thin layers with interbedded sands and shales.

Even though the standard ray method is known for its inaccuracy in describing wave propagation in such complex media and its inability to describe the entire acoustic or elastic wavefield compared with full-wave methods, ray methods still occupy a primary position in many seismic applications. The reasons are probably that ray methods generally are very fast compared to wavefield-continuation techniques. In addition, ray tracing has an event-oriented nature, which means that specific arrivals of elementary waves (e.g., transmitted P- and S-waves, primary PP and PS reflected waves for selected horizons, multiples, etc.) can be labeled in synthetic seismograms or in computed sets of Green's function attributes.

Many papers on geophysics address the issue of extending the standard ray method to overcome some of the difficulties mentioned earlier and yet retain the advantages related to efficiency and elementary wave labeling. Among such extensions are the Gaussian beam method (Červený et al., 1982; Popov, 1982; Hill, 1990, 2001), the Maslov method (Chapman and Drummond, 1982; Kendall and Thompson, 1993), and the asymptotic theory of diffractions (Klem-Musatov et al., 1994). See also Chapman (2002, 2004) and Červený et al. (2007), where other references can be found.

The main objective of this tutorial paper is to discuss and demonstrate certain modern applications of ray tracing. In contrast to prior references, we follow a different strategy for enhancing the applicability of the standard ray method. Rather than requiring further development of this specific method, we consider any ray-tracing-based process as one element in a composite system of processes that, as a whole, is able to yield better results than standard ray tracing applied alone. As we show in a number of examples, our strategy can result in useful methods. One motivating factor has been to design the composite processes in a way suitable for modern software design, in accordance with the suggestions of Rueger (2004). In addition to defining composite systems of process elements, the model of elastic parameters is decomposed into local and global elements. An important part of the strategy is to define rules for the interaction of process elements with model elements. In particular, if a process element based on the standard ray method is to be applied to a given model element, one must ensure that this model element has been properly prepared, e.g., by smoothing.

The three main sections following this introduction describe methodology, examples, and conclusions. Our main focus is on the examples section, which demonstrates certain composite seismic modeling techniques that have been developed specifically to meet the demands of practical applications in the petroleum industry. However, these composite processes are still firmly based on the standard ray method as an ingredient of the wavefront-construction method. The common idea is not only to produce synthetic prestack seismograms but also to directly model quantities that correspond to processed seismic data or attributes derived from processed seismic data, such as those being mostly used by seismic interpreters.

METHODOLOGY

In this section we give an overview of the underlying methodology. For brevity, we refer to the model of elastic parameters as "the model." In particular, we describe an approach for decomposition of the model and a number of composite processes in which the standard ray method is one of the constituents.

Model elements and process elements

A basic assumption for all composite methods considered in this paper is that the model can be decomposed into one main (global) element of wide extent and one or several distinct local elements (Figure 1). The local elements can be volumes (layers, blocks), surfaces (boundaries, horizons, interfaces, reflectors), or a combination. Often, the global element is a smooth volume of the model. This global volume element is allowed to have a general shape and is commonly referred to as the background or overburden model, depending on the context. However, our methodology is not limited to global volume elements that are smooth throughout; if ray tracing is to be performed in a background model, several modeling scenarios will benefit, including continuous layers separated by continuous interfaces.

One of the advantages is the possibility of simulating reflected waves. An important point in this context is to ensure that elastic parameter functions in the layers and functions specifying the interfaces (marked as A and B in Figure 1) are appropriate for standard ray tracing, which must satisfy certain general validity criteria (Červený, 2001). A smooth volume element is considered acceptable for ray tracing if the elastic properties do not vary significantly within the prevailing wavelength. Similarly, a surface element of the model is classified as acceptable for ray tracing if it does not contain sharp edges and vertices and if the data points for the surface element have a regular distribution on the scale of the wavelength.

For illustration, Figure 1 shows some rays traced between an arbitrary point in the background model and the surface. Local reflectivity properties, e.g., direction-dependent reflection coefficients, can be associated with local surface elements not included in the background model (marked C and D in Figure 1). This association can be done independently of the elastic properties of the background model, which are typically of a macro nature.

Given the previous decomposition into model elements, we propose a strategy where standard ray tracing is used in combination with other methods, thus increasing the applicability of ray tracing. An important part of the strategy is to introduce additional techniques, i.e., process elements, in the processing of very complex model elements, for which the standard ray method is inappropriate. Besides improving the applicability of standard ray tracing, the purpose is effective software design. Examples of process elements are finite-difference modeling of wave propagation within a volume element, numerical integration over a surface element using the Kirchhoff integral, simulating the depth migration result on a target horizon, and simulated imaging related to a local volume, typically a target zone. One special processing operation related to a model element actually makes the element suitable for standard ray tracing by smoothing and other editing operations. This process element differs from the others in that it changes the model.

FD modeling in a local volume element

In FD modeling, the model is commonly represented by regular grids of the elastic parameters (Virieux, 1986). Although FD modeling is usually considered to be a complete wave-simulation approach, it is an expensive process, especially when running realistic 3D surveys and repeated experiments. Given this background, Lecomte et al. (2004) proposes a hybrid approach combining ray tracing and FD modeling in a three-step process, where the connection between ray tracing and FD modeling is done at a given coupling surface. In the context of model decomposition into global and local elements, FD modeling is applied naturally to a local volume element where standard ray tracing is inappropriate, e.g., a complex target zone, whereas ray tracing is applied in the background model.

Integration over a local surface element

Assume that a certain target reflector has been classified as a local surface element of the model. The two-way seismic response for a given source point, receiver point, and recording time can then be obtained by approximate Kirchhoff modeling, which may be formulated as a wave-type specific integral (Hilterman, 1975; Trorey, 1977; Frazer and Sinton, 1984; Frazer and Sen, 1985; Eaton and Clarke, 2000; Schleicher et al., 2001). The numerical integration can be implemented in various ways. For example, Spencer et al. (1997) propose an efficient algorithm using triangulated surfaces. The algorithm integrates over stripes within the triangles, assuming that traveltimes and other attributes can be interpolated linearly.

Green's function attributes contributing to the Kirchhoff surface integral commonly are calculated by standard ray tracing in a background model. Moreover, computed seismograms include the effects of reflections as well as diffractions from the given target reflector. In this manner, Kirchhoff modeling can be regarded as a composite approach serving to extend the applicability of standard ray tracing.

Simulating the migration amplitude on a local surface element

In survey planning and illumination studies, the principal objective often is to model the seismic response of a given target reflector in the depth domain. In particular, when the overburden geology is complex, e.g., with salt structures between the acquisition level and the reservoir zone, it is of special interest to try to simulate the target response for given survey geometries, sailing directions, etc. (Laurain et al., 2004a).

If a 3D modeling system able to produce terabytes of synthetic prestack seismograms is available, these data can be fed into a processing system to produce a final processed (e.g., depth-migrated) seismic cube in the target area, in the same way as for real data from a seismic acquisition. Seismic amplitude maps can then be derived for the target horizon(s). However, this is a time-consuming and cumbersome process, especially as making a change in the model or survey geometry requires another full loop of that modeling/processing workflow. Reducing such costs was the motivation for developing the simulated migration amplitude method (Figure 2), which is described in some detail in Laurain et al. (2004b).

The method produces synthetic migrated amplitude maps on target horizons directly from the modeled ray attributes for a given 3D survey. First, the full 3D survey is simulated by two-way wavefront

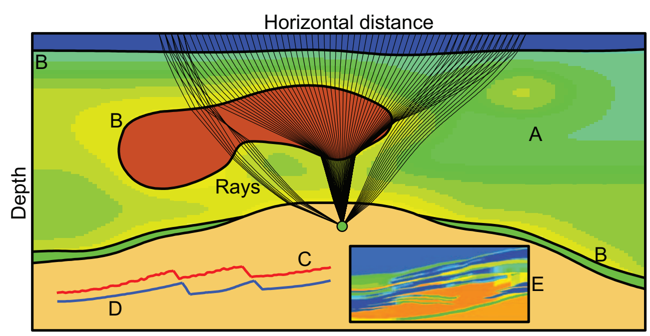

Figure 1. Model decomposition into global and local elements. Global element, or background model, consisting of a combination of smooth volume (A) and surface elements, i.e., smooth layers and interfaces (B). Two local surface elements (C and D), not belonging to the background model, are superimposed: the upper (C) is corrugated, and the lower (D) is piecewise smooth but contains edge points corresponding to faulting. Reflectivity properties, e.g., direction-dependent reflection coefficients, can be associated with the local surface elements, independently of the background model. Also shown is a volume element (E) not in the background model, with realistic velocity variations corresponding to a complex region (model courtesy of the Statoil-sponsored SVALEX project). Rays are shown in the background model between an arbitrary point (green dot) and the surface. Colors of volume elements indicate variation in P-wave velocity. These colors are not comparable for global and local elements.

construction, producing events with associated attributes. Typically, several hundred thousand shots can be simulated in parallel on a standard Linux cluster, generating several hundred million events. Second, the migration simulation process loops over all (or selected) events. Each event, which would contribute to a wavelet on a prestack seismogram, is instead contributing to a migrated amplitude event on the known target reflector.

Given an input wavelet and the necessary ray attributes of a reflected event, the migration simulation process calculates how this pulse would contribute to a Kirchhoff migrated amplitude, but only exactly on the target reflector where the amplitude map is to be calculated. To achieve this, an approximation for the so-called isochron, i.e., the surface of constant two-way traveltime, is established in the neighborhood of the reflection point. In a complete Kirchhoff migration, this isochron is calculated inherently from volume-type Green's functions, whereas the migration simulation method uses an approximation valid in the Fresnel zone around the known reflection point. The function representing the isochron corresponds to a second-order approximation of the two-way traveltime in the vicinity of the reflection point. By mapping the events only around the known reflection points, the migration simulation process becomes much more efficient than a conventional migration applied to synthetic data. In this way, the process acts as a perfect parsimonious migration (Hua and McMechan, 2003) or Fresnel-volume migration (Luth et al., 2005).

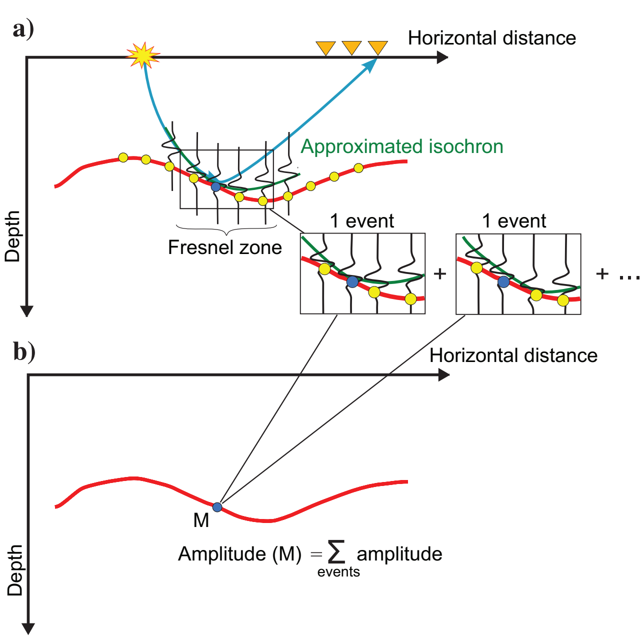

Figure 2. Concept of simulated migration amplitudes. (a) As an initial step, forward modeling by ray tracing is performed in a 3D model for a specific survey and a given target reflector. The forward modeling yields a number of events that are used for computing synthetic trace data. For each event, the synthetic trace is smeared on an approximated isochron with lateral extension defined according to the Fresnel zone. (b) The amplitude at a point M on the target reflector is obtained by summing contributing amplitudes of individual events.

Simulating prestack images in a local volume element

In the case of complex detailed reservoir models, the validity limits of standard ray tracing may not allow proper modeling. One possible solution in such cases is to define the reservoir zone as a local volume element and then use the hybrid ray-tracing/FD approach. However, this method only generates synthetic seismograms, which must be processed, e.g., by time or depth migration, to yield useful results for further analyses. Although this workflow represents a practical compromise between a time-consuming but complete FD modeling and a faster but less accurate ray-tracing modeling, its cost is still significant, especially considering the need for subsequent processing.

Therefore, a different approach has been developed, where prestack depth migration (PSDM) images of the reservoir can be generated very efficiently without generating synthetic traces and processing them (Lecomte et al., 2003; Lecomte and Pochon-Guerin, 2005; Lecomte, 2006; U. S. patent pending). This local PSDM simulator has its roots in a generalized diffraction tomography algorithm for inhomogeneous media (Hamran and Lecomte, 1993; Lecomte, 1999) and its recent reformulation (Lecomte et al., 2005) as a repeated local imaging process using the fast Fourier transform (FFT). The local PSDM simulator needs direction-dependent reflectivity grids for the local target model as input and acts as an image processor by filtering such grids in the wavenumber domain. The final simulated PSDM image in the depth domain is obtained after taking an inverse FFT of the filtered result. Assuming a local plane-wave approximation, the filters are specified in the wavenumber domain (Gelius et al., 2002). The scattering wavenumber vector $\mathbf{k}_{sr}$ is obtained at a given image point from incident and scattered slowness vectors, computed by ray tracing (Figure 3). Thereby, one can obtain source/receiver parameters and ray attributes (traveltime, amplitude, polarization, directivity, etc.) to be used as weight factors in the filters.

Simulation of local prestack images represents another composite method that includes calculating Green's function attributes by the standard ray method. The attributes are calculated as for a conventional Kirchhoff prestack depth migration process. Thus, for this

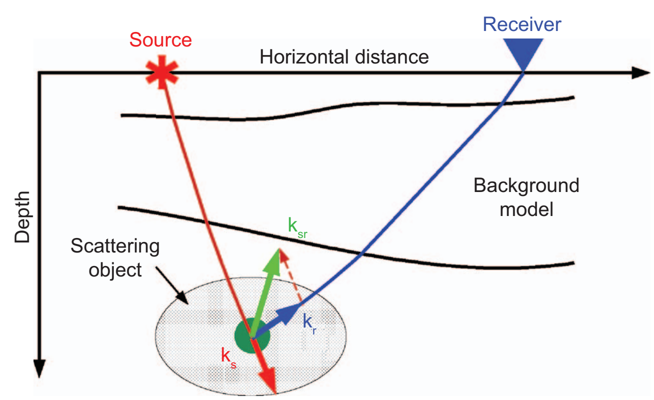

Figure 3. Concept of simulated local imaging. Slowness vectors at a given point (green dot) in a scattering object for a source ray (red) and a receiver ray (blue) yield corresponding wavenumber vectors $\mathbf{k}_s$ and $\mathbf{k}_r$. The scattering wavenumber vector $\mathbf{k}_{sr}$ is calculated from the equation $\mathbf{k}_{sr} = \mathbf{k}_r - \mathbf{k}_s$. A background model is used for the ray tracing. This model may contain interfaces in the overburden part but must be smooth within the volume covered by the scattering object.

composite method, the standard ray method is used in the global volume element, the background model, whereas a local image processing technique is applied to a local volume element, referred to in this context as a scattering object. As a consequence, the background model must be specified and prepared in such a way that the requirements for ray tracing are satisfied.

Kirchhoff imaging in a local or global volume element

In the framework of this paper, Kirchhoff imaging and data-mapping techniques (Hubral et al., 1996; Tygel et al., 1996; Bleistein et al., 2001; Bleistein and Gray, 2001), conventionally applied to a global model, are considered as composite methods. The basic components are preparation of the model, which means to make it acceptable for ray tracing; a ray-based algorithm to obtain Green's function attributes; and the specific imaging/data-mapping algorithm, e.g., PSDM by diffraction stack (Hubral et al., 1996). We especially emphasize the potential in designing the imaging algorithm to accommodate multiarrivals (see, e.g., Gray et al., 2002).

EXAMPLES

A number of examples illustrate the methodology described earlier. First, we show the results of a tutorial where the response from a local surface element is modeled in different ways. Thereafter, the composite methods yielding simulated migration amplitudes on a local surface element and simulated images in a local volume element are applied to simple, as well as highly realistic, models. One of the models is based on real data interpretation. Finally, we present an example of conventional Kirchhoff PSDM by diffraction stack applied to an anisotropic model.

Tutorial example: Modeling the response from a local surface element

We present a series of very simple modeling examples to demonstrate the basic principles, limitations, and differences among selected approaches. In these examples, we keep the background velocity field constant and focus on the shape of a local surface element because this factor causes the most problems in practical applications.

Consider the model in Figure 4, referred to as model A. It consists of one single horizon made of four planes dipping only in the inline direction, intersecting each other along sharp edges. The P-wave velocities above and below the horizon are 2000 and 2500 m/s, respectively; the P-/S-wave velocity ratio is two; and density is 2.5 g/cm^3 throughout. Just for illustration, we display wavefronts at several time steps for both downgoing and reflected P-waves, propagating toward a chosen receiver line. Note that all wavefront construction calculations are performed in three dimensions, even though the following examples show simulations only for models that are constant in the crossline direction.

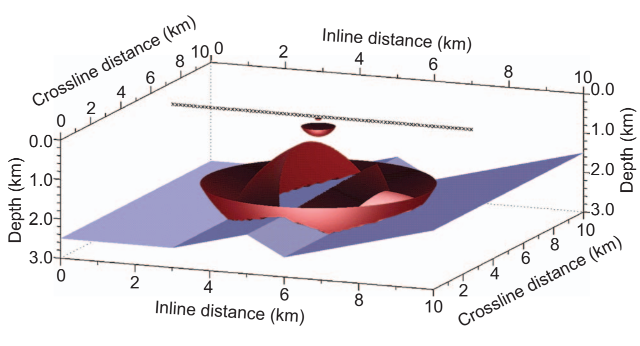

Figure 4. Model A with shotpoints and wavefronts superimposed.

Now consider a zero-offset survey in the inline direction of model A with a shot/receiver spacing of 50 m. Figure 5a shows raypaths resulting from 3D wavefront construction; Figure 5b exhibits the resulting synthetic seismograms consisting of four separate branches, one for each horizon plane. In this and the following examples, a 20-Hz zero-phase Ricker wavelet was used as the source pulse.

A seismic interpreter knows that in practice, even for such a simple model, the reflected wavefield is not that simple. An FD simulation in the same model gives the seismic section of Figure 5c. The gaps between the specular reflections, satisfying Snell's law, are filled with wave energy known as edge diffractions, which the standard ray method does not account for automatically.

Figure 6a shows a cross section of a slightly modified model (B), where we have performed a careful smoothing of the edges to turn the four planes into one horizon with continuous dip. The synthetic seismograms from ray tracing in Figure 6b show that the gaps have been filled with diffraction-like registrations created from the parts of the horizons with large curvature. Although these registrations are from reflected events, the amplitudes are much smaller than those from the plane portions because of large geometric spreading. Other typical deficiencies that can be observed in ray-tracing-based seismograms are some unrealistically high amplitudes close to the cusps of the caustics and the lack of a gradual decay in the form of diffracted energy, as can be observed from the comparison with FD seismograms in Figure 6c.

The conclusion from this small experiment is that sharp edges on a surface can be smoothed slightly to produce a diffraction-like ray-tracing response, which is closer to reality than keeping them sharp. This also can be illustrated by migrating the seismic sections from the sharp and smooth model (Figure 7). The sharp model response

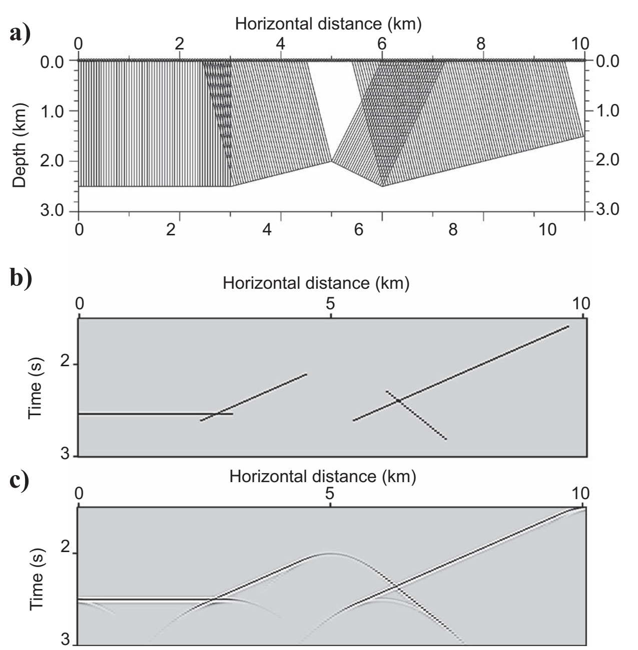

Figure 5. Experiment using model A. (a) Rays and seismograms calculated by (b) ray tracing and (c) FD method.

shows more distinct artifacts around the edges, whereas migration in the smooth model better collapses the edges, resulting from the presence of diffraction-like energy.

These simple examples show that ray tracing may give plausible results if the relevant local model elements are prepared properly by smoothing, resampling, etc., in such a way that the superlocal calculation along the single rays also is representative within a Fresnel volume. Another simple example illustrates a case where this assumption is unfulfilled. We have constructed some small ripples in a certain area of the horizon (Figure 8). Because of the lack of smoothness, the rays and the resulting seismograms in Figure 8b show unrealistic amplitude fluctuations, also leading to a poor reconstruction of the horizon in the migrated results of Figure 8c.

Many years of experience with using ray tracing in practical cases have taught us that the lack of smoothness of the model horizons is a major source of inaccuracy. Horizons typically are imported from an interpretation database, and they may be quite corrugated, especially if autotrackers have been applied. To find a proper smoothing compromise for ray tracing is not straightforward: too little smoothing means fluctuating and unstable amplitudes, too much smoothing can destroy details that the seismic waves can see with the given frequency. The question is whether we can apply the ray method in a more robust way, i.e., to make it respond better to sharper details of the model horizons.

To illuminate this subject, we use ray tracing in combination with the Kirchhoff integral. Figure 9a-c shows synthetic seismograms calculated by Kirchhoff modeling for our three models, A, B, and C. Time migration was applied to the section in Figure 9c and is shown in Figure 9d. The Kirchhoff modeling method automatically simulates edge diffractions and is much more stable than standard ray tracing with respect to model ripples. The reason is that the amplitude response is obtained as a sum over the horizon and the process thus does not possess the superlocal behavior of ray tracing. Disregarding some minor artifacts related to the sampling, the time-migrated image in Figure 9d shows a very good reconstruction of the horizon, as compared to Figure 8c.

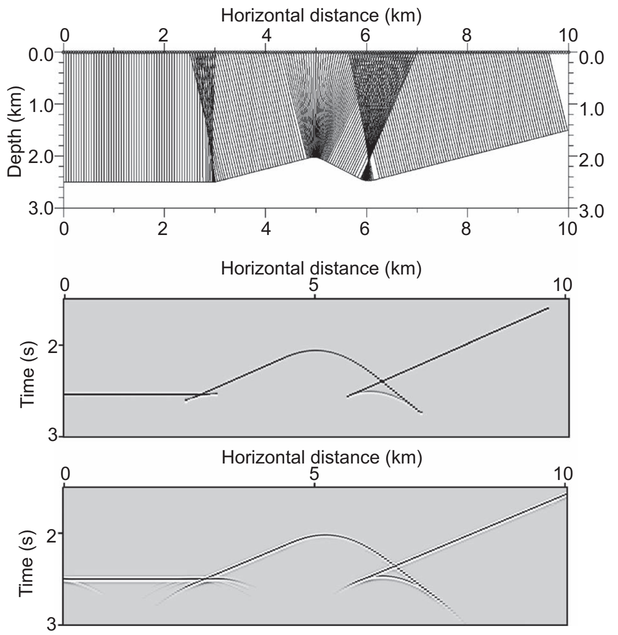

Figure 6. Experiment using model B. (a) Rays, and seismograms calculated by (b) ray tracing and (c) FD method.

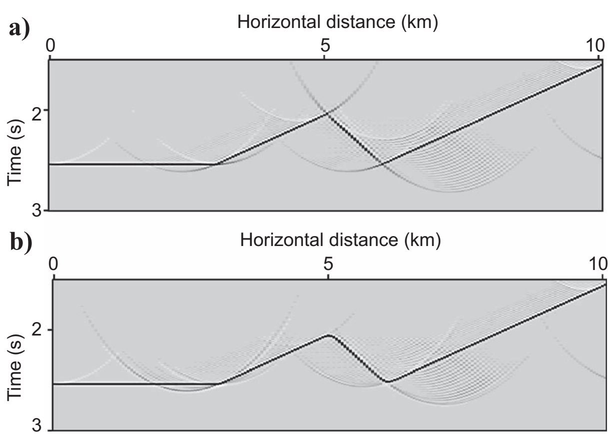

Figure 7. Time-migrated ray tracing seismograms from models (a) A and (b) B.

Simulation of migration amplitude on a target reflector

As a first illustration, we apply the method for simulating migration amplitudes to a target reflector separating two layers of constant velocities (Kaschwich and Mispel, 2006). The velocity values are 2000 and 2500 m/s above and below the reflector, respectively, but the density is constant in the entire model. A common shot survey is specified, with 120 shots located between 2 and 8 km in the inline direction (shot spacing 50 m). The source pulse is a zero-phase Ricker wavelet with a central frequency of 20 Hz. Source/receiver offsets have ranges between 0 and 1 km, and the receiver spacing is 25 m.

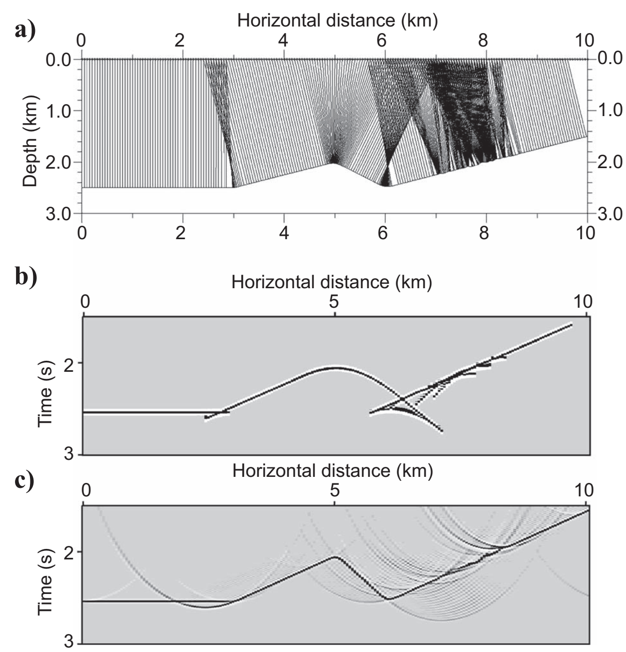

Figure 8. Experiment using model C. (a) Rays, (b) ray-tracing seismograms, and (c) time-migrated ray-tracing seismograms.

A synthetic seismic data set was generated using ray tracing. This data set was subsequently depth migrated, and migration amplitudes were extracted along the reflector. Thereafter, the same survey and model setup were used to simulate migration amplitude on the target reflector by the method described in the methodology section. Figure 10a and b shows simulated migration amplitude results based, respectively, on the full survey and on a few selected single events. Because of the large separation of the reflection points for these single events, one can clearly observe the Fresnel-zone imprints on the target reflector. Figure 10a represents the sum of all single-event results. Amplitude profiles corresponding to PP and PS reflections, for the complete prestack depth migration and the migration simulation method, are shown in Figure 11. For comparison, the result of a conventional illumination analysis (e.g., Sassolas et al., 1999; Bear et al., 2000; Laurain, 2004b) is also included. The curves for the simulated amplitude (red) and the complete PSDM amplitude (green) are very consistent, whereas the illumination amplitude (blue) is typically higher and lower, respectively, at crests and valleys of the target reflector.

In a second experiment, a realistic model was constructed with the goal of demonstrating the potential of ray tracing in analyzing seismic illumination properties related to a subsurface target. The model is shown in Figure 12 and consists of eight depth-domain interfaces from seabed down to base reservoir with a velocity field assigned to each layer. The target reflector is located at about 2–3 km depth, covering an area of about 100 km^2, and constitutes the upper boundary of a reservoir formation including three local highs assumed to contain oil. The properties of the brine- and water-filled parts of the reservoir were modeled using standard rock-physics relationships.

The goals of the illumination analysis were to determine whether the oil can be detected using a 3D marine seismic survey, investigate the seismic sampling of the target, and analyze the uncertainties in determining the lateral extent of the prospects. For these purposes, a complete 3D seismic survey was modeled using a single source vessel towing eight streamers. The separation between the streamers was 100 m. The streamer length was limited to 4000 m with 50-m receiver spacing and the first receiver located 200 m from the source. The source-point interval was 50 m along lines separated by a distance of 400 m, totaling about 6000 shots for this survey.

The modeling results are summarized in terms of the previously described simulated migration amplitude maps. As is common for standard illumination maps, the modeled event attributes are sorted in regular bin cells covering the target reflector and analyzed statistically within each cell. The simulated migration amplitude map in Figure 13a defines the location of those oil pockets having significantly stronger amplitudes than the surrounding brine-saturated formation. However, some variability resulting from overburden and target geometry is visible. Figure 13b shows the number of reflection points (hits) per bin cell, demonstrating, as in Figure 11, the well-known effect that hits accumulate at the crests and become more scattered in the valleys, thus causing an irregular seismic sampling of the target. Figure 13c shows the maximum horizontal distance between the common reflection point (CRP) and the common midpoint (CMP), which is the minimum migration aperture required in seismic migration algorithms. This parameter also depends on the target topography, and its value may become several thousands of meters.

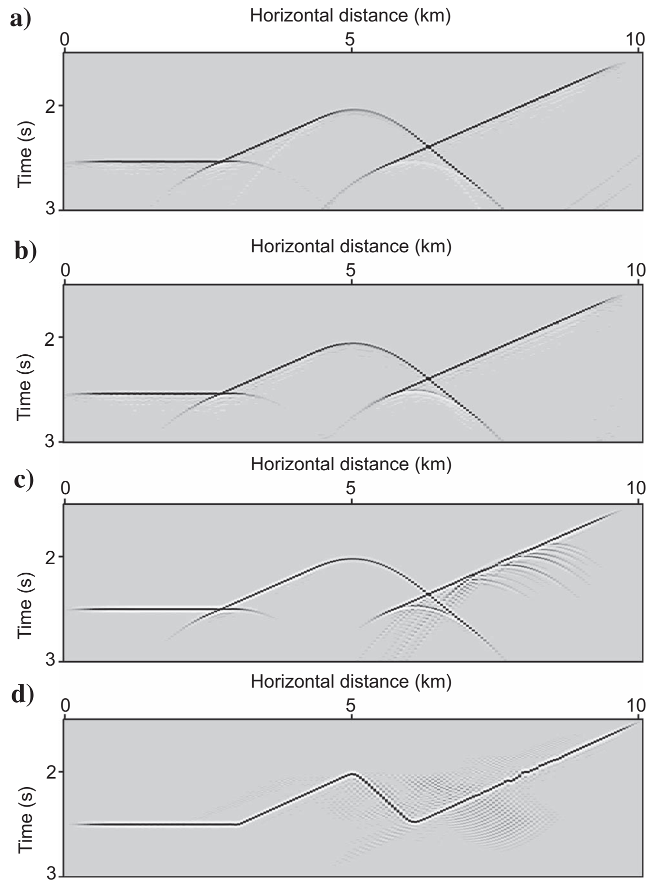

Figure 9. Kirchhoff modeling seismograms for models (a) A, (b) B, and (c) C. (d) Time-migrated image of the section in (c).

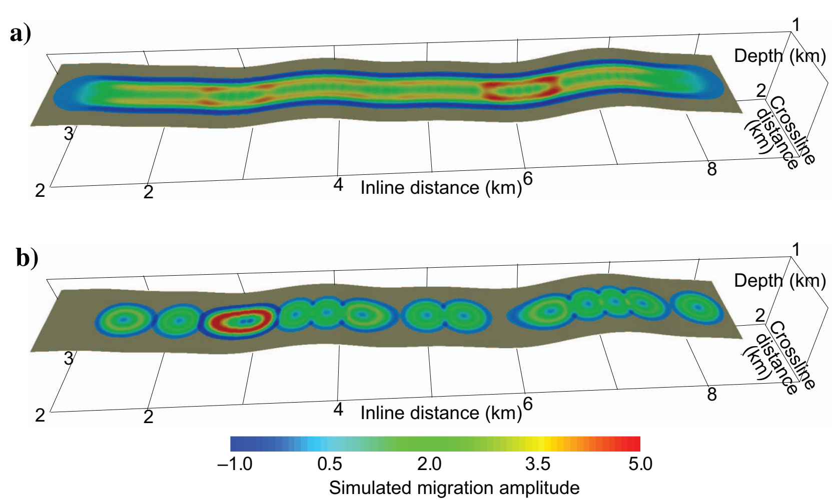

Figure 10. Maps of simulated migration amplitudes corresponding to (a) the complete common-shot survey and (b) a few shot-receiver pairs (zero offset).

Simulated local imaging applied to a reservoir model

In this subsection, we show results obtained by a specific modeling workflow designed for 4D analysis (Drottning et al., 2005, 2006), using the simulated local imaging concept described previously. The input to the workflow is a real Eclipse reservoir model of the Norne field (Osdal et al., 2006) and additional rock/well information.

Rock-physics modeling allows one to estimate corresponding elastic parameters, which can be used, in turn, to calculate reflectivity grids by Zoeppritz or any amplitude variation with offset/amplitude variation with analysis (AVO/AVA) formulas (Figure 14a). Another type of input comes from ray tracing, which is used to calculate appropriate filters in the scattering wavenumber domain. These fil-

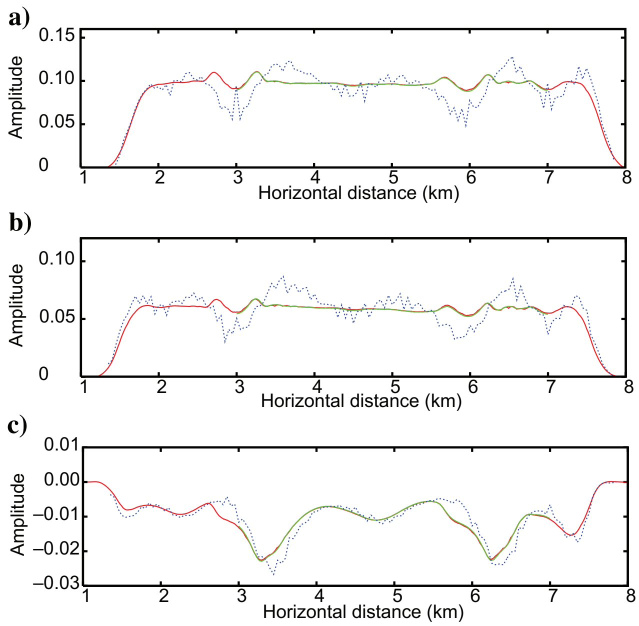

Figure 11. Amplitudes along reflector for (a) PP reflection, (b) PS reflection, horizontal component, and (c) PS reflection, vertical component.

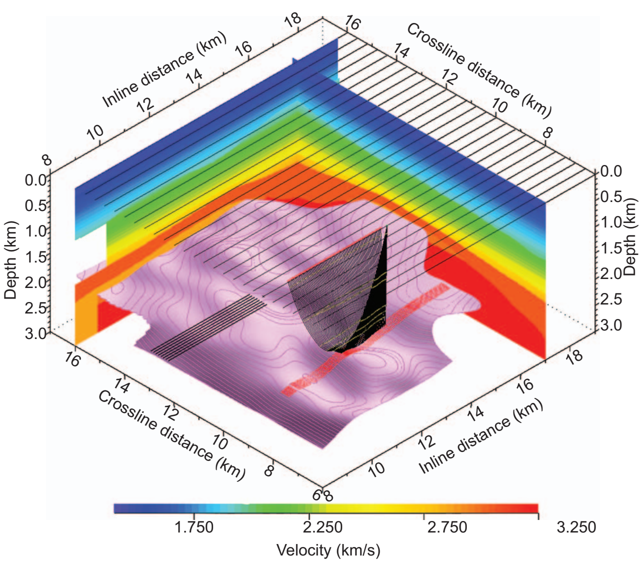

Figure 12. Target reflector with 25-m equidistance between depth contours and the velocity field for the illumination analysis. Shown are shot lines of the marine survey and streamers associated with the first shot of line 7, rays associated with another shot and one central streamer, and reflection points (red) on the target reflector for selected shots along line 7.

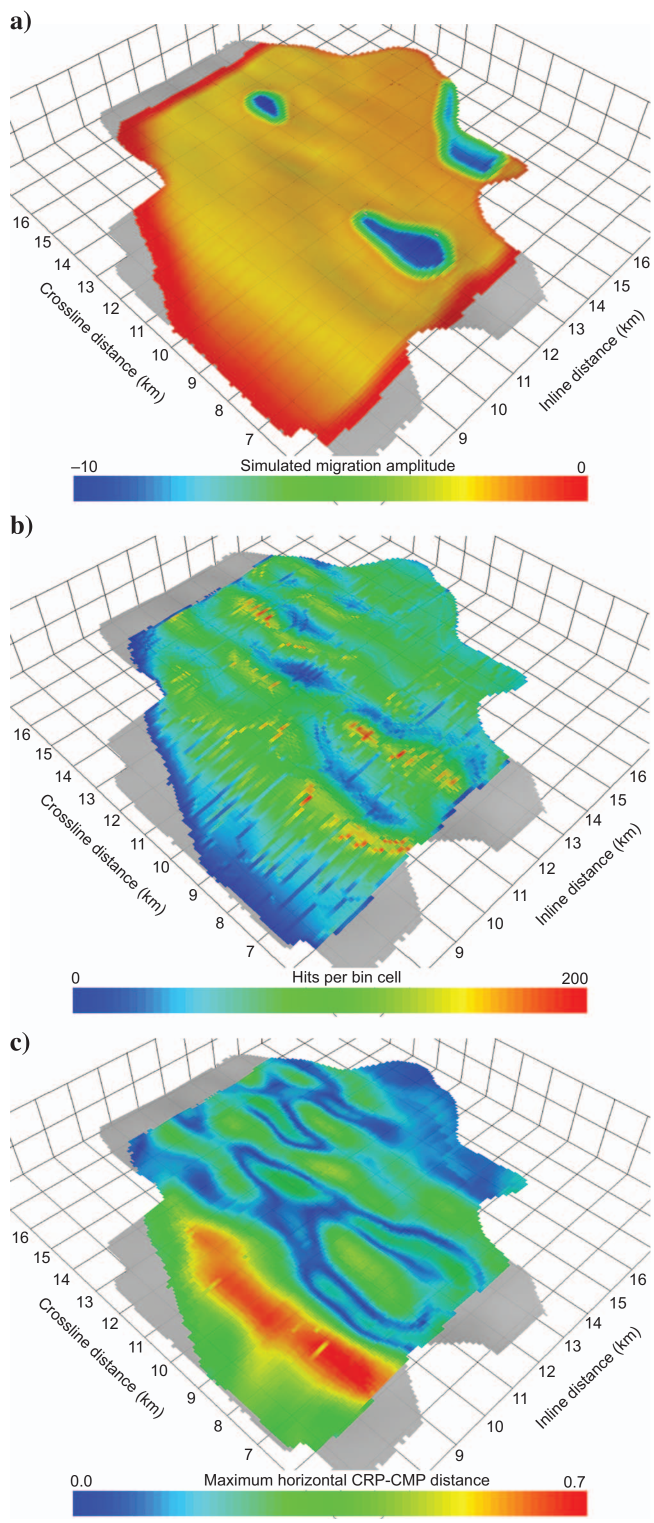

Figure 13. Illumination maps generated for the target reflector. (a) Simulated migration amplitude. (b) Number of hits per bin cell. (c) Maximum horizontal CRP-CMP distance.

ters were built here for a given overburden model, a 20-Hz zero-phase Ricker wavelet, incident and scattered P-waves, and one marine survey. Figure 14b shows a simulated PSDM section, obtained when using only a zero-offset acquisition configuration. The resolution is good, especially horizontally, and the steep faults, which yield clear contrasts, are well illuminated.

On the contrary, Figure 14c shows a simulated PSDM section for a constant offset of 4 km, where both lateral resolution and illumination are worse in comparison. This is easily explained by the survey geometry because shotpoints in this case are not located far enough toward the right side of the structure. The limited aperture effect would be easily corrected by a longer profile, but this example shows that the PSDM simulator takes into account such limited resolution and illumination effects automatically. It is important to emphasize that it was sufficient to use ray directions from only one reference point in the reservoir zone to make the filters in the scattering wavenumber domain. The simulated prestack data are obtained directly in the depth domain, but depth-to-time conversion can be applied to get corresponding prestack data in the time domain. Various ray-tracing methods are available for this purpose.

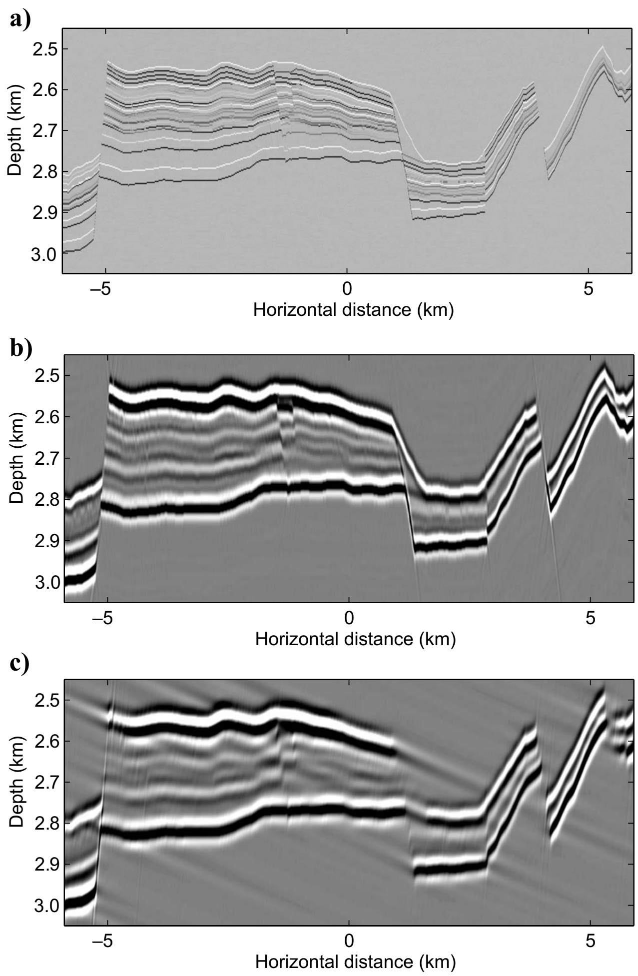

Figure 14. Norne model. (a) Reflectivity grid from Eclipse model and rock properties, the values varying from about –0.1 (white) to about +0.1 (black). (b) Simulated local depth-migrated image for a constant offset of 0 km. (c) Simulated local depth-migrated image for a constant offset of 4 km.

Imaging tilted anisotropic structures

Figure 15 illustrates a case where an anisotropic model is needed to obtain an accurate depth-migration image from a synthetic seismic data set. The anisotropy parameters, epsilon and delta, and the density are given in Table 1. The model consists of a salt structure and several adjacent transversely isotropic (TI) shale layers where the axis of symmetry is normal to the bedding (Figure 15b). For this type of model where the axis of a TI medium varies continuously from point to point, ray tracing has been performed conventionally using a formulation including 21 elastic parameters (Červený, 1972; Gajewski and Pšenčik, 1987). We use a ray-tracing approach based on continuously rotating a local anisotropy coordinate system

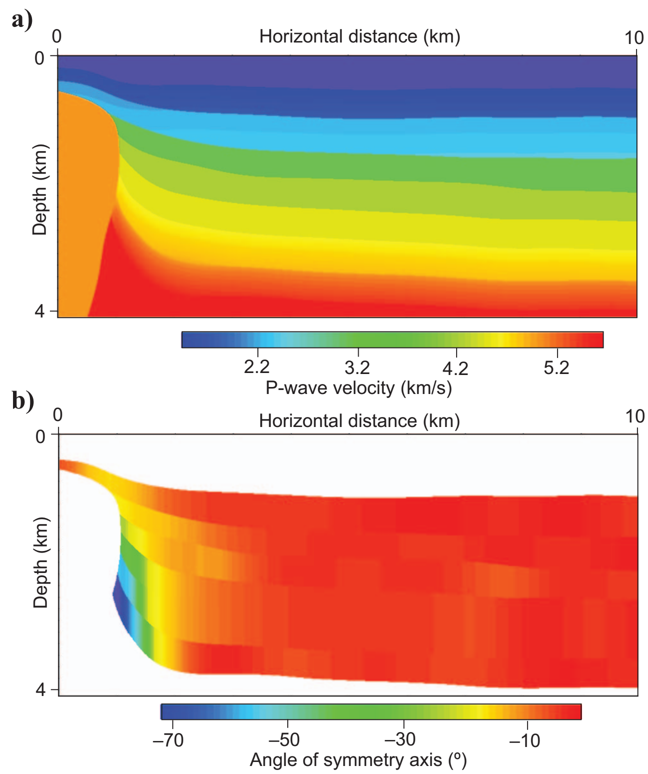

Figure 15. (a) Salt model and (b) angle of the symmetry axis.

Table 1. Anisotropy parameters and density for the given salt model (Figure 15).

Rock	Epsilon	Delta	Density
Water			1.000
Isotropic sediments			2.000
Pierre shale	0.015	0.060	2.250
Anisotropic shale	0.103	–0.001	2.340
Green river shale	0.195	–0.226	2.175
Shale	0.200	–0.075	2.420
Mesaverde shale	0.128	0.078	2.680
Mesaverde mudshale	0.034	0.211	2.520
Basalt			2.600
Salt			2.200

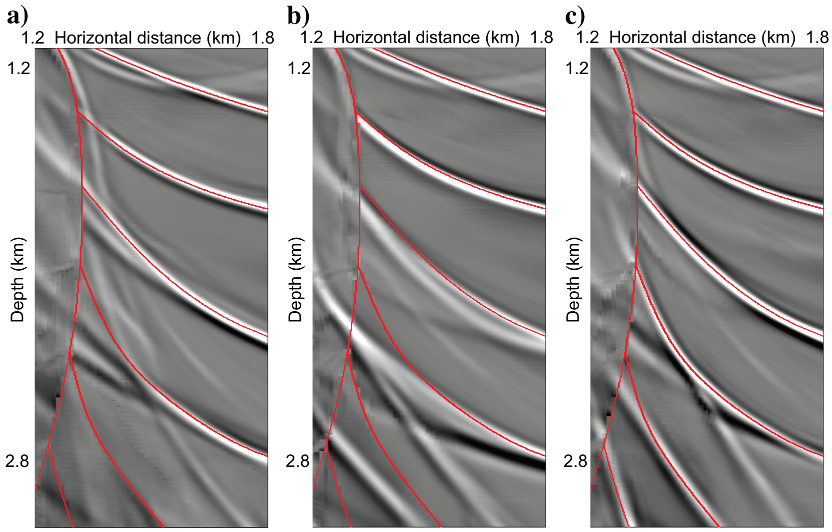

Figure 16. Depth-migrated image obtained using (a) the ISO model, (b) the VTI model, and (c) the TTI model.

(Iversen and Pšenčik, 2007). Thereby, the number of elastic parameters of influence reduces to five or less, which leads to considerable savings from more efficient calculations and reduced consumption of computer memory. In addition, one is guaranteed that the anisotropic symmetry is retained when interpolating between elastic parameters in different locations.

In the terminology introduced previously, the model in Figure 15 consists of a number of local volume elements (layers). An important step of a composite imaging procedure is smoothing the various elastic properties of these volume elements. The model resulting after the smoothing procedure is referred to here as the tilted transversely isotropic (TTI) model, whereas the corresponding models with a vertical symmetry axis (VTI) and zero anisotropy (ISO) in all layers.

Using the TTI model, we generated a synthetic seismic data set by ray tracing. Imaging results for all three models are shown in Figure 16. The image for the VTI model shows a misfit for all displayed reflectors, in particular for the lower part. For the isotropic model, the lower two reflectors are poorly imaged. A good subsurface image in the vicinity of the salt dome is obtained only when using the TTI model. However, this image can be improved additionally by using a full-wave approach for synthetic data generation, multiarrivals for migration, a model that is smooth throughout, and enhanced muting and other preprocessing steps before migration.

CONCLUSIONS

A major challenge in the development of ray-tracing technology is to achieve more robust applications of the ray method at the various stages of the seismic value chain — from acquisition to time-lapse interpretation. One may select a strategy based specifically on extending the validity area of the standard ray method itself, or one may follow the focus of this paper, which is to consider ray tracing as only one constituent of a composite system of processes.

With the help of simple modeling examples, thus avoiding too many interfering effects obscuring the results, we have tried to demonstrate the true nature of the standard ray method, particularly with respect to amplitude calculations. A general conclusion is that proper model preparation is crucial to gain stable, reliable results. Smoothing of horizons is the most critical point because horizons produced by the seismic interpretation process often may show rapid small fluctuations.

The combination of the standard ray method with the wavefront construction method serves a variety of purposes, e.g., simulating large realistic 3D surveys and modeling the reflected wavefield for predefined targets and wave modes, as well as efficient generation of Green's function attributes needed for real data imaging, simulated local imaging, and Kirchhoff modeling. The last technique turns out to be a very interesting candidate for effectively extending the limits of ray theory because it dramatically reduces the need for reflector smoothness, thereby modeling both edge and caustic diffractions. Although more time consuming, performing Kirchhoff modeling in 3D is feasible today by having an efficient wavefront construction tracer running in parallel, even on small clusters.

Moreover, composite techniques combining ray tracing in a background model and other techniques in a much more complex target zone have turned out to be useful approaches for generating synthetic seismic data belonging to the time and depth domains. In particular, the fast and flexible local PSDM simulator is a very powerful process for reservoir and time-lapse studies, where synthetic seismic cross sections or 3D cubes can be generated interactively when making changes in the model. For survey planning and illumination studies, where one wants just an overall reflection response of a given target reflector, it is more practical and efficient to simulate migration amplitude maps on the fly directly from the ray tracing results than to generate cubes of synthetic traces.

ACKNOWLEDGMENTS

We thank our colleagues at NORSAR in the Seismic Modeling department who contributed to the development and applications of the presented methods, in particular, Ketil Åstebøl, the main architect behind the 3D model-building technology. We acknowledge Mike Branston for valuable assistance with internal review and figure editing. Special thanks also go to our past colleagues, Vetle Vinje (now at CGG) and Renaud Laurain (now at PGS), for their important contributions to wavefront construction modeling and simulation of migration amplitudes. The reviews by two anonymous referees and Sam Gray were highly appreciated. The FD modeling code of the NUCLEUS software of PGS has been used by Renaud Laurain for some of the examples. The authors also thank Statoil for permission to use the Eclipse model of the Norne reservoir and to show the results. The Seismic Unix package has been used for processing and display of data in the tutorial example. This work has received support over several years from the Research Council of Norway.

REFERENCES

Aki, K., and P. G. Richards, 1980, Quantitative seismology: Theory and methods, vol. I: W. H. Freeman & Co.

Bear, G., C.-P. Lu, R. Lu, D. Willen, and I. Watson, 2000, The construction of subsurface illumination and amplitude maps via ray tracing: The Leading Edge, **19**, 726–727.

Bleistein, N., J. K. Cohen, and J. W. Stockwell Jr., 2001, Mathematics of multidimensional seismic imaging, migration, and inversion: Springer Pub. Co., Inc.
Bleistein, N., and S. H. Gray, 2001, From the Hagedoorn imaging technique to Kirchhoff migration and inversion: Geophysical Prospecting, **49**, 629–643.
Červený, V., 1972, Seismic rays and ray intensities in inhomogeneous anisotropic media: Geophysical Journal of the Royal Astronomical Society, **29**, 1–13.
———, 2001, Seismic ray theory: Cambridge University Press.
Červený, V., and F. Hron, 1980, The ray series method and dynamic ray tracing system for three-dimensional inhomogeneous media: Bulletin of the Seismological Society of America, **70**, 47–77.
Červený, V., L. Klimeš, and I. Pšenčik, 2007, Seismic ray method: Recent developments, *in* R.-S. Wu and V. Maupin, eds., Advances in wave propagation in heterogeneous earth: Academic Press, 1–126.
Červený, V., I. A. Molotkov, and I. Pšenčík, 1977, Ray method in seismology: Charles University, Prague.
Červený, V., M. M. Popov, and I. Pšenčík, 1982, Computation of wave fields in inhomogeneous media — Gaussian beam approach: Geophysical Journal of the Royal Astronomical Society, **70**, 109–128.
Červený, V., and J. E. P. Soares, 1992, Fresnel volume ray tracing: Geophysics, **57**, 902–915.
Chapman, C. H., 2002, Seismic ray theory and finite frequency extensions, *in* International handbook of earthquake and engineering seismology, part A: Academic Press, 103–123.
———, 2004, Fundamentals of seismic wave propagation: Cambridge University Press.
Chapman, C. H., and R. Drummond, 1982, Body-wave seismograms in inhomogeneous media using Maslov asymptotic theory: Bulletin of the Seismological Society of America, **72**, S277-S317.
Drottning, Å., T. A. Johansen, J.-A. Skjervheim, and S. Aanonsen, 2005, Seismic response of fluid flow in a layered permeability model: 67th Annual Conference and Exhibition, EAGE, Extended Abstracts, P106.
Drottning, Å., I. Lecomte, H. Gjøystdal, A. Skorstad, O. Kolbjørnsen, and O. Huseby, 2006, Modelling the seismic response to production: A closer look at the sensitivity to overburden, survey, rock physics model and seismic modelling approach: Biennial Geophysical Seminar, Norwegian Petroleum Society (NPF), Extended Abstracts, 69–72.
Eaton, D. W., and G. Clarke, 2000, A Kirchhoff integral method to model 3-D elastic wave scattering: 70th Annual International Meeting, SEG, Expanded Abstracts, 2472–2475.
Frazer, L. N., and M. K. Sen, 1985, Kirchhoff-Helmholtz reflection seismograms in a laterally inhomogeneous multi-layered elastic medium — I. Theory: Geophysical Journal of the Royal Astronomical Society, **80**, 121–147.
Frazer, L. N., and J. B. Sinton, 1984, A Kirchhoff method for the computation of finite-frequency body-wave synthetic seismograms in laterally inhomogeneous media: Geophysical Journal of the Royal Astronomical Society, **78**, 413–429.
Gajewski, D., and I. Pšenčik, 1987, Computation of high-frequency seismic wavefields in 3-D laterally inhomogeneous anisotropic media: Geophysical Journal of the Royal Astronomical Society, **91**, 383–411.
Gelius, L.-J., I. Lecomte, and H. Tabti, 2002, Analysis of the resolution function in seismic prestack depth imaging: Geophysical Prospecting, **50**, 505–515.
Gibson, R. L., V. Durussel, and K.-J. Lee, 2005, Modeling and velocity analysis with a wavefront-construction algorithm for anisotropic media: Geophysics, **70**, no. 4, T63–T74.
Gjøystdal, H., E. Iversen, R. Laurain, I. Lecomte, V. Vinje, and K. Åstebøl, 2002, Review of ray theory applications in modelling and imaging of seismic data: Studia Geophysica et Geodaetica, **46**, 113–164.
Gray, S., C. Notfors, and N. Bleistein, 2002, Imaging using multiarrivals: Gaussian beams or multiarrival Kirchhoff?: 72nd Annual International Meeting, SEG, Expanded Abstracts, 1117–1120.
Hamran, S.-E., and I. Lecomte, 1993, Local plane-wavenumber diffraction tomography in heterogeneous backgrounds. Part I: Theory: Journal of Seismic Exploration, **2**, 133–146.
Hill, N. R., 1990, Gaussian beam migration: Geophysics, **55**, 1416–1428.
———, 2001, Prestack Gaussian beam migration: Geophysics, **66**, 1240–1250.
Hilterman, F. J., 1975, Amplitudes of seismic waves — A quick look: Geophysics, **40**, 745–762.
Hua, B., and G. A. McMechan, 2003, Parsimonious 2D prestack Kirchhoff depth migration: Geophysics, **68**, 1043–1051.
Hubral, P., J. Schleicher, and M. Tygel, 1996, A unified approach to 3-D seismic reflection imaging, part I: Basic concepts: Geophysics, **61**, 742–758.
Iversen, E., J. Mispel, R. Laurain, and V. Vinje, 2005, Zero-offset modelling and simulated migration by one-way wavefront construction: 67th Annual Conference and Exhibition, EAGE, Extended Abstracts, P263.
Iversen, E., and I. Pšenčík, 2007, Ray tracing for continuously rotated local coordinates belonging to a specified anisotropy: Studia Geophysica et Geodaetica, **51**, 37–58.
Iversen, E., V. Vinje, and L.-J. Gelius, 1996, Raytracing in a smooth velocity model: Journal of Seismic Exploration, **5**, 129–140.
Kaschwich, T., and J. Mispel, 2006, Simulated migration amplitudes of converted waves: First results: 76th Annual International Meeting, SEG, Expanded Abstracts, 2574–2578.
Kendall, J.-M., and C. J. Thompson, 1993, Maslov ray summation, pseudocaustics, Lagrangian equivalence and transient seismic waveforms: Geophysical Journal International, **113**, 186–214.
Klem-Musatov, K. D., F. Hron, and L. Lines, eds., 1994, Theory of seismic diffractions: SEG.
Lambaré, G., P. S. Lucio, and A. Hanyga, 1996, Two-dimensional multivalued traveltime and amplitude maps by uniform sampling of ray field: Geophysical Journal International, **125**, 584–598.
Laurain, R., L.-J. Gelius, V. Vinje, and I. Lecomte, 2004a, A review of 3D illumination studies: Journal of Seismic Exploration, **13**, 17–37.
Laurain, R., V. Vinje, and C. Strand, 2004b, Simulated migration amplitudes: Improving amplitude estimates in seismic illumination studies: The Leading Edge, **23**, 240–245.
Lecomte, I., 1999, Local and controlled prestack depth migration in complex areas: Geophysical Prospecting, **47**, 799–818.
———, 2006, Fremgangsmåte for simulering av lokale prestakk dypmigrerte seismiske bilder: Norwegian patent 322 089.
Lecomte, I., H. Gjøystdal, and Å Drottning, 2003, Simulated prestack local imaging: A robust and efficient interpretation tool to control illumination, resolution, and time-lapse properties of reservoirs: 73rd Annual International Meeting, SEG, Expanded Abstracts, 1525–1528.
Lecomte, I., H. Gjøystdal, Å. Drottning, F. Maaø, T. A. Johansen, and R. Bakke, 2004, Efficient and flexible modelling of reservoirs: The HybriSeis concept: The Leading Edge, **23**, 432–437.
Lecomte, I., S.-E. Hamran, and L.-J. Gelius, 2005, Improving Kirchhoff migration with repeated local plane-wave imaging? A SAR-inspired signal-processing approach in prestack depth imaging: Geophysical Prospecting, **53**, 767–785.
Lecomte, I., and L. Pochon-Guerin, 2005, Simulated 2D/3D PSDM images with a fast, robust, and flexible FFT-based filtering approach: 75th Annual International Meeting, SEG, Expanded Abstracts, 1810–1813.
Luth, S., S. Buske, R. Giese, and A. Goertz, 2005, Fresnel volume migration of multicomponent data: Geophysics, **70**, no. 6, S121–S129.
Mispel, J., and P. Williamson, 2001, 3D wavefront construction for P and SV waves in transversely isotropic media: 63rd Annual Conference and Exhibition, EAGE, Extended Abstracts, P094.
Osdal, B., O. Husby, H. A. Aronsen, N. Chen, and T. Alsos, 2006, Mapping the fluid front and pressure buildup using 4D data on Norne field: The Leading Edge, **25**, 1134–1141.
Popov, M. M., 1982, A new method of computation of wave fields using Gaussian beams: Wave Motion, **4**, 85–97.
Rueger, A., 2004, Aspects of modern raytracing application design: Studia Geophysica et Geodaetica, **48**, 143–165.
Sassolas, C., G. Lescoffit, and P. Nicodeme, 1999, The benefits of 3-D ray tracing in acquisition feasibility: 69th Annual International Meeting, SEG, Expanded Abstracts, 629–632.
Schleicher, J., M. Tygel, B. Ursin, and N. Bleistein, 2001, The Kirchhoff-Helmholtz integral for anisotropic, elastic media: Wave Motion, **34**, 353–364.
Spencer, C. P., C. H. Chapman, and J. E. Kragh, 1997, A fast, accurate integration method for Kirchhoff, Born and Maslov synthetic seismogram generation: 67th Annual International Meeting, SEG, Expanded Abstracts, 1838–1841.
Trorey, A. W., 1977, Diffractions for arbitrary source-receiver locations: Geophysics, **42**, 1177–1182.
Tygel, M., J. Schleicher, and P. Hubral, 1996, A unified approach to 3-D seismic reflection imaging, part II: Theory: Geophysics, **61**, 759–775.
Vinje, V., E. Iversen, K. Åstebøl, and H. Gjøystdal, 1996a, Estimation of multivalued arrivals using wavefront construction, part I: Geophysical Prospecting, **44**, 819–842.
———, 1996b, Estimation of multivalued arrivals using wavefront construction, part II: Tracing and interpolation: Geophysical Prospecting, **44**, 843–858.
Vinje, V., E. Iversen, and H. Gjøystdal, 1993, Traveltime and amplitude estimation using wavefront construction: Geophysics, **58**, 1157–1166.
Virieux, J., 1986, P-SV wave propagation in heterogeneous media: Velocity-stress finite-difference method: Geophysics, **49**, 1933–1957.